Thermo-responsive viscoelastic wormlike micelle to elastic hydrogel transition in dual-component systems

Yiyang Lin, Yan Qiao, Yun Yan and Jianbin Huang*

Received 7th April 2009, Accepted 22nd May 2009
First published as an Advance Article on the web 3rd July 2009
DOI: 10.1039/b906960g

In this work, we report a thermo-responsive phase transition from a viscoelastic wormlike micelle solution to an elastic hydrogel in a mixture of an imidazole-type surfactant, 1-hexadecyl-3-methylimidazolium bromide (C_{16}MIMBr), and sodium salicylate (NaSal). Above the critical temperature T_{gel}, the sample exhibits characteristic wormlike micelle features with strong viscoelastic properties. As the temperature was lowered below the T_{gel}, the viscoelastic solution transforms into an elastic hydrogel with a remarkable elastic modulus increase. Polarization microscopy, SEM, and XRD were employed to reveal the morphology and molecular arrangement of the organized microstructures in the hydrogel. The unexpected phase transition from viscoelastic solution to hydrogel can be attributed to the crystallization of wormlike micelles, which is related to the strong synergic interaction between the surfactant and hydrotrope.

Introduction

Molecular self-assembly provides a powerful tool for the creation of well-organized structures in the nanometre or micrometre length scale, such as micelles, vesicles, fibers, discs and tubes.[1–5] Surfactant solutions represent a well-documented class of self-assembled systems that can offer diverse organized structures.[6–8] Above the critical micelle concentration (CMC), hydrophilic surfactants form small globular micellar aggregates and the solutions show Newtonian flow behavior. Under certain conditions such as concentration, salinity, temperature, presence of counterions, *etc.*, the globular micelles may undergo uniaxial growth and form very long and highly flexible aggregates, referred to as "wormlike" or "threadlike" micelles.[9–16] Above a threshold concentration c^*, wormlike micelles may entangle into a transient network, which displays remarkable viscoelastic properties. The rheological behavior observed for wormlike micelles in the surfactant solution is similar to that for flexible polymers, and therefore, aqueous solutions of entangled wormlike micelles are often called "living polymer systems". The research of wormlike micelles has drawn considerable interest owing to their superior properties and wide applications.[17–20] Viscoelastic wormlike micelles or threadlike micelles have been observed in various surfactant systems, including mixtures of cationic and anionic surfactants,[21–23] nonionic surfactants,[24–26] zwitterionic surfactants[27–29] and ionic surfactants with different additives.[30–34]

Hydrotropes were found to promote the formation of viscoelastic wormlike micelles in ionic surfactant solutions, in which the surfactant interacts strongly with hydrotrope due to electrostatic attraction and hydrophobic effect.[30–34] Salicylate, tosylate, chlorobenzoate, hydroxynaphthalenecarboxylates, and nitrobenzoate (all containing an aromatic group) were reported to induce wormlike micelle formation in a cationic surfactant solution. Unlike surfactant molecules, hydrotropes are a class of amphiphilic compounds that cannot form well-organized structures, such as micelles, but do increase the solubility of organic molecules in water by several orders of magnitude.[35] The common structural characteristics of hydrotropes are the coexistence of an unsaturated hydrocarbon ring and an ionic group within one molecule. Strong synergistic effects are often observed when hydrotropes are added to aqueous surfactants or polymer solutions. In particular, various hierarchically self-assembled structures such as tubes, ribbons, vesicles and lamellar structures can be fabricated in mixtures of surfactants and hydrotropes.[36–40]

Despite the number of studies dedicated to the investigation of surfactant–hydrotrope mixtures, most of the work has mainly concentrated on the structure–property relationship of various hydrotropes in typical surfactant solutions such as cetyltrimethylammonium bromide (CTAB) and cetylpyridinium bromide (CPyBr). Reports on the systems of novel surfactants and hydrotropes are less considered in the literature. Recently, Wattebled and Laschewsky explored the synergistic effect of aromatic hydrotropes on the characteristic solution properties of ammonium gemini surfactants.[41] Our group investigated the structural evolution of gemini surfactant (12-2-12) with the addition of a hydrophobic counterion. Surprisingly, we observed rich aggregate morphologies in such systems.[42] It seems that by using surfactants with novel structures, unexpected phenomena might be encountered in the mixed systems of surfactant–hydrotropes.

For these reasons, we are motivated to explore the novel surfactant system of 1-hexadecyl-3-methylimidazolium bromide (C_{16}MIMBr) and sodium salicylate (NaSal). These two compounds were selected mainly due to the following considerations. Firstly, the alkyl-3-methylimidazolium cation is structurally similar to those found in ionic liquids which are

Beijing National Laboratory for Molecular Sciences (BNLMS), College of Chemistry and Molecular Engineering, Peking University, Beijing, 100871, China. E-mail: jbhuang@pku.edu.cn; Fax: +86-10-62751708; Tel: +86-10-62753557

known as "green solvents". The investigation of the imidazolium-type surfactant is, therefore, of great importance from both the practical and academic points of view.[43–45] Secondly, we intend to introduce π–π interaction between the salicylate anion and the imidazolium cation in the surfactant–hydrotrope mixture, which may bring unexpected effects to the self-assembled behavior in the surfactant system. Indeed, we observed an unusual thermo-responsive transition between viscoelastic wormlike micelles and elastic hydrogels in this novel surfactant–hydrotrope mixed system. Normally, viscoelastic wormlike micelles may experience an exponential increase of characteristic lengths with lowering temperature which leads to an increase in rheological properties. To the best of our knowledge, the thermo-responsive transition from viscoelastic wormlike micelle to elastic hydrogel has not yet been reported. In this paper, the aggregate transition induced by temperature was systematically investigated, and the origin of phase transition and structural evolution was further discussed.

Experimental and materials

Materials

Cetyltrimethylammonium bromide (CTAB) and cetylpyridinium bromide were products of A. R. grade of Beijing Chemical Co. and recrystallized five times from acetone and ethanol before use. Alkyl-3-methylimidazolium bromide was synthesized and purified according to ref. 43. Other compounds were of A. R. grade.

Rheological measurements

The rheological properties of samples were measured with a ThermoHaake RS300 rheometer. Cone and plate geometries were used in each case. The temperature was controlled at 25 ± 0.05 °C. A solvent trap was used to minimize water evaporation. Frequency spectra were recorded in the linear viscoelastic regime of the samples, as determined from dynamic strain sweep measurements. For the steady-shear experiments, sufficient time was allowed before data collection at each shear rate so as to ensure that the viscosity reached its steady-state value.

Maxwell model

The Maxwell model is a simple model used to describe the rheological properties, which constitute a single spring connected in series to a viscous element (dashpot). In shear experiments, G' (the elastic modulus) and G'' (the loss modulus) are given

$$G'(\omega) = \frac{G_0(\omega\, t_R)^2}{1 + (\omega\, t_R)^2} \quad (1)$$

$$G''(\omega) = \frac{G_0\omega\, t_R}{1 + (\omega\, t_R)^2} \quad (2)$$

Here, G_0 is the plateau modulus, and t_R is the relaxation time estimated as $1/\omega_c$ where ω_c is the crossover frequency at which G' and G'' intersect. The "Cole–Cole" plot of G'' *versus* G' reveals the semicircle characteristic of a Maxwell fluid, which is expressed as eqn (3)

$$G''^2 + \left(G' - \frac{G_0}{2}\right)^2 = \left(\frac{G_0}{2}\right)^2 \quad (3)$$

XRD measurements

Self-supported cast films for the X-ray diffraction (XRD) studies were prepared by dispersing the sample solutions in precleaned quartz slides above the gel temperature. Then the sample was allowed to stay below the gel temperature for more than three hours. After that the sample was quickly frozen in liquid N_2 and subsequently freeze-dried under vacuum with a freeze-dryer. Reflection XRD studies were carried out with a model XKS-2000 X-ray diffractometer (Scintaginc). The X-ray beam was generated with a Cu anode, and the wavelength of the KR1 beam was 1.5406 Å. The X-ray beam was directed toward the film edge, and the scanning was done up to the 2θ value of 10°.

Differential scanning calorimetry (DSC)

The DSC measurements were carried out at 1 °C min^{-1} using a Micro DSC III (Setaram-France) instrument.

Polarization microscopy

Photographs of birefringence were taken by a polarization microscope (OLYMPUSBH-2) with Kodak-400 color film.

SEM observations

The microstructures of the samples were studied by field-emission scanning electronic microscopy (SEM, Hitachi FE-S4800). In order to detect the morphology of the organization the hydrogel was quickly frozen in liquid N_2 and subsequently freeze-dried under vacuum with a freeze-dryer.

Results and discussion

Viscoelastic wormlike micelle formation in solutions of C_{16}MIMBr–NaSal mixtures

Before the addition of NaSal, the C_{16}MIMBr solution is a transparent micellar solution. Upon the addition of NaSal, the viscosity gradually increases, which is indicative of micelle elongation. To further identify the structural transition, rheological measurements were carried out. Fig. 1a shows the steady-shear viscosity of the sample with variation of NaSal concentration in a 40 mM C_{16}MIMBr solution. The sample viscosity exhibits a significant increase with the addition of NaSal. It is known that increasing salt concentration initially results in an increase in the curvature energy for surfactant aggregates. This leads to an increase in micellar length and the formation of wormlike micelles. As the NaSal concentration is further increased, the zero-shear viscosity exhibits a well-defined maximum. The decrease of viscosity is generally explained as a decrease of the micellar contour length[46] or as the formation of branched micelles.[47–49]

Dynamic rheological measurements were further applied to characterize the flowing behavior. Fig. 1b shows the elastic modulus G' and viscous modulus G'' varying with oscillation frequency. It can be noted that the sample exhibits strong

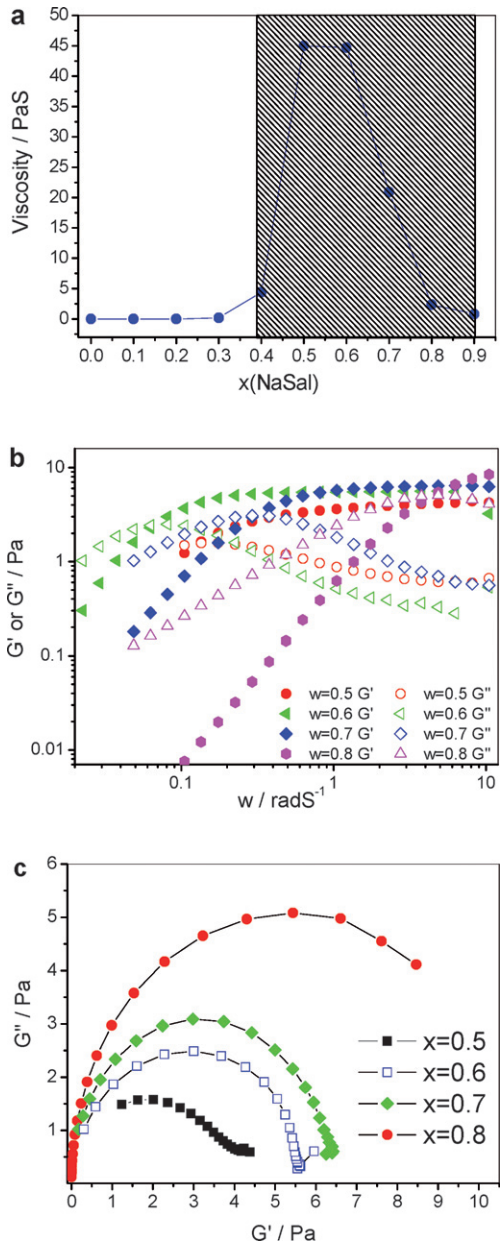

Fig. 1 (a) Zero-shear viscosity of the 40 mM C_{16}MIMBr solution with different amounts of NaSal. The shadow zone depicts the formation of viscoelastic solution; (b) G' and G'' *versus* frequency for 40 mM C_{16}MIMBr solutions with different NaSal concentrations; (c) Cole–Cole plots for 40 mM C_{16}MIMBr solutions with different NaSal concentrations.

viscoelastic properties with the addition of NaSal and the modulus exhibits a good fit to a single-relaxation-time Maxwell model. Meanwhile, the "Cole–Cole" plot of G'' *versus* G' (Fig. 1c) reveals the semicircle characteristic of a Maxwell fluid.

In summary, all these results suggest the structural evolution from a spherical micelle to a wormlike micelle in the C_{16}MIMBr system upon the addition of NaSal.

Reversible thermo-responsive sol–gel transition

Interestingly, the C_{16}MIMBr–NaSal system undergoes an extraordinary transition from viscoelastic wormlike micelle solution to an elastic hydrogel when lowering the temperature. Fig. 2 shows the macroscopic appearance of the sol–gel transition in the system of 40 mM C_{16}MIMBr and 28 mM NaSal solution. At temperatures above 20 °C, the sample is transparent and fluid. When the temperature lowered below 20 °C, it became opalescent immediately (Fig. 2b) and can be turned upside down without any flow in a 1 cm diameter test tube (Fig. 2c). Herein, the temperature 20 °C is defined as gel temperature or T_{gel} for this sample.

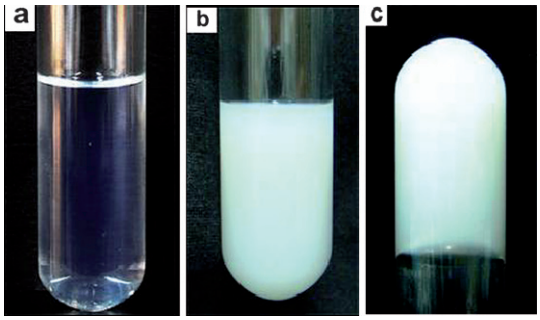

Fig. 2 Macroscopic appearance of the isotropic solution to opalescent gel transition at different temperatures: (a) 21 °C; (b) 20 °C; (c) 20 °C upside down.

To evaluate the viscoelastic properties of sol–gel transition, we used a dynamic stress sweep to determine the linear viscoelastic regime for the dynamic frequency sweep. As shown in Fig. 3a, both the storage modulus (G') and the loss modulus (G'') are independent of stress from 0.1 to 10 Pa (with G' dominating G''), indicating that the sample is an elastic hydrogel. Also from

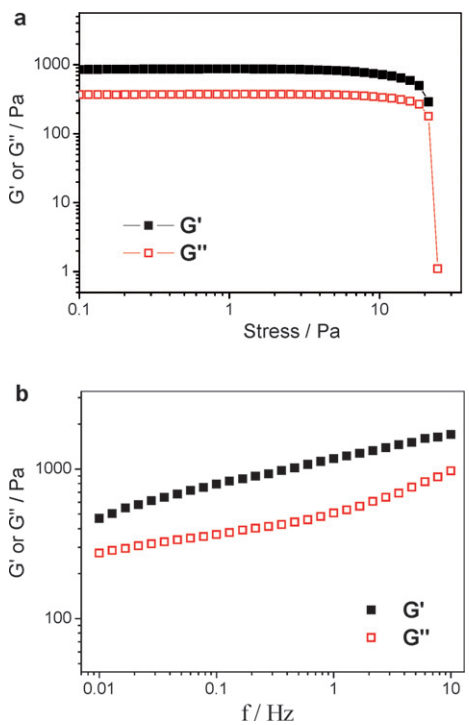

Fig. 3 (a) Dynamic stress sweep of the gel at a frequency of 1 Hz ($T = 20$ °C). (b) Elastic modulus G' and viscous modulus G'' as functions of frequency ($T = 20$ °C).

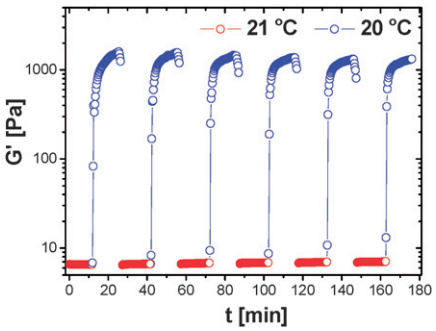

Fig. 4 Repeated thermo-sensitive sol–gel transition over six cycles.

Fig. 3a, it can be clearly seen that the hydrogel is stable under a 10 Pa stress. After setting the stress at 1 Pa within the linear response regime, we used a dynamic frequency sweep to study the hydrogel. As shown in Fig. 3b, the storage modulus G' and the loss modulus G'' slightly increase with the increase of frequency from 0.01 to 10 Hz. The value of G' is always larger than that of G'' in the whole range (0.01–10 Hz), suggesting that the hydrogel is fairly tolerant to external force. Fig. 4 shows the repeated thermo-sensitive sol–gel transition. It is clear that the storage modulus G' undergoes an abrupt jump over two-orders of magnitude. More importantly, the thermo-responsive visco-elastic fluid to elastic gel transition can be reversibly repeated simply by heating or cooling. Even after six cycles, both the shear modulus and the macroscopic appearance are recovered completely.

To clarify the temperature-dependent sol–gel transition in more detail, we performed differential scanning calorimetry (DSC) measurements on a C_{16}MIMBr–NaSal solution (Fig. 5). The cooling curve shows a sharp exothermic peak from 20 to 18 °C. The onset of gelation at 20 °C agrees with the result of rheological measurements. A large transition enthalpy can be observed. The heating curve was also presented in Fig. 5. A major transition with the largest latent heat is seen at 21 °C. The slight shift of the peak may result from the time delay of the phase transition. It is worth noting that the molar transition enthalpies in heating and cooling cycles are close to each other. This indicates that the sol–gel transition is fully reversible under heating or cooling.

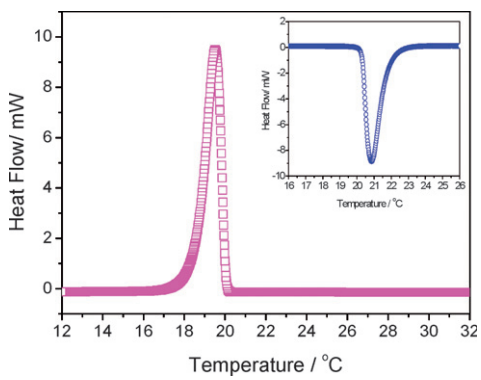

Fig. 5 DSC curves obtained for a 40 mM C_{16}MIMBr and 28 mM NaSal solution undergoing a cooling process. The inset is the representative curve of the same sample under heating.

Microscopic architectures of the C_{16}MIMBr–NaSal hydrogel

The sol–gel transition induced by temperature is a macroscopic manifestation of microstructural evolution upon temperature stimulus. To understand the assembled structure of C_{16}MIMBr–NaSal from a microscopic point, scanning electron microscopy (SEM) images of 40 mM C_{16}MIMBr and 28 mM NaSal were recorded. Fig. 6 depicts the SEM image of a xerogel of C_{16}MIMBr–NaSal below the T_{gel}. Cylindrical structures appear to be the main architectures in this system. The width of the rods ranges from 1 to 2 μm. It is, therefore, understandable that water molecules are immobilized in a network of these cylindrical structures, which finally result in the hydrogel formation.

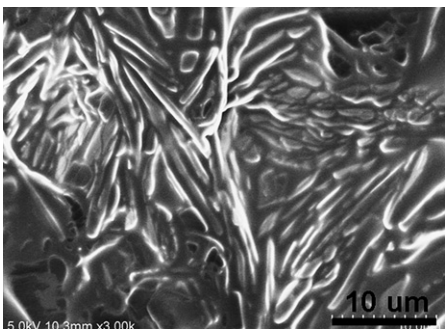

Fig. 6 SEM image of the 40 mM C_{16}MIMBr and 28 mM NaSal hydrogel at 20 °C.

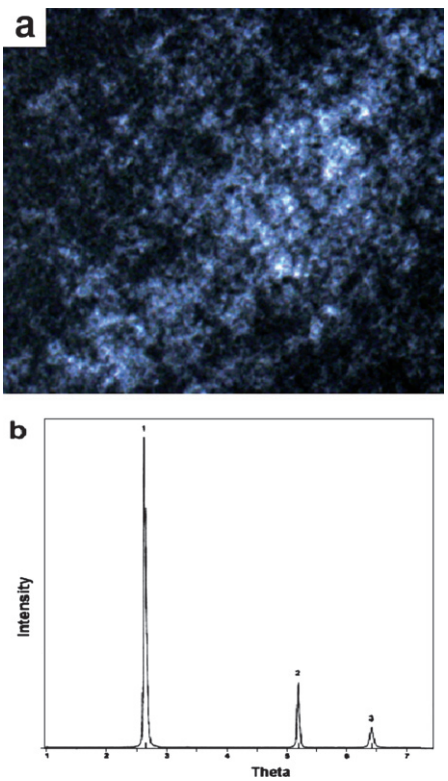

Fig. 7 (a) Photograph of a 40 mM C_{16}MIMBr and 28 mM NaSal hydrogel through a polarization microscope at 20 °C; (b) XRD spectrum of a xerogel of the C_{16}MIMBr–NaSal system.

Although the SEM images do not show the fine structure of the rods, the thickness indicates that the rods are superstructures. Also, the texture of hydrogel was also studied under a polarization microscope. Birefringence phenomenon can be observed (Fig. 7a) which confirms the existence of unaxial structures in the hydrogel.

To examine the molecular packing in the cylindrical structure of the hydrogel, small angle X-ray diffraction was employed for the xerogel of the C_{16}MIMBr–NaSal system. As shown in Fig. 7b, the XRD spectrum of xerogel in the C_{16}MIMBr and NaSal system exhibits sharp reflection peaks demonstrating a highly ordered molecular packing in the hydrogel. In addition, the X-ray diffraction patterns of the xerogels show 1 : 1/2 : 1/3 periodical reflection peaks, indicating a lamellar organization of the molecules in the hydrogel. The obtained spacings (d) of the xerogels correspond to 3.30 nm, which is less than twice the extended molecular length of C_{16}MIMBr (2.30 nm, by MM2 force field simulation), but larger than the length of one molecule. This indicates that the hydrogel may maintain an interdigitated bilayer structure with a thickness of 3.3 nm (Fig. 8a). It could be also possible that tilted multilayer structures are formed (Fig. 8b).

In both pictures, the electrostatic attraction, hydrophobic interactions and π–π stacking cooperatively induce the self-assembly of C_{16}MIMBr and NaSal, in which salicylate anion was strongly binding to the surfactant's imidazolium headgroup (Fig. 8a and 8b). Such molecular arrangements in surfactant–hydrotrope mixtures have been well established in previous literature.[50–52]

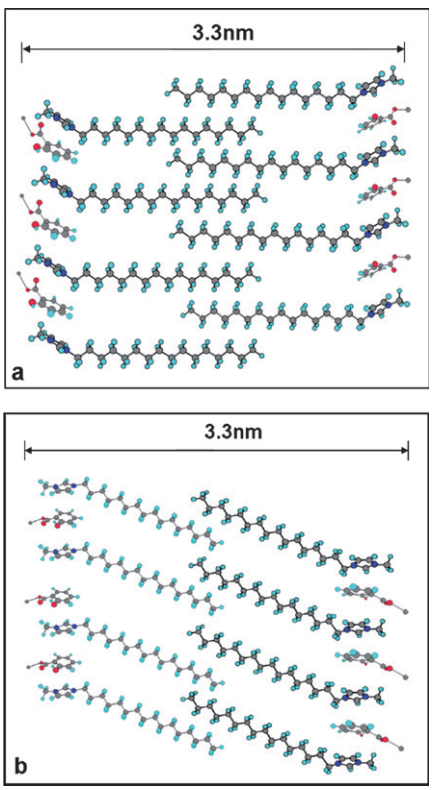

Fig. 8 Possible molecular packing in the mixture of C_{16}MIMBr and NaSal: (a) interdigitated structure; (b) tilted structure.

The origin of thermo-responsive viscoelastic fluid–hydrogel transitions

Typically, when a wormlike micellar solution is cooled, the micellar contour length increases exponentially with temperature. The reason for this is that, at lower temperatures, surfactant monomers can exchange slower between the cylindrical body and the hemispherical end-cap of the wormlike micelle. Thus, because the end-cap constraint is severe at lower temperatures, the wormlike micelles grow to a larger extent. The increase in micellar length leads to an exponential increase in rheological properties such as the zero-shear viscosity η_0 and the relaxation time t_R.

However, in this paper, we report an unexpected trend in the rheological behavior for certain wormlike micellar solutions as a function of temperature. Instead of increasing exponentially, the viscoelasticity experiences a dramatic jump upon cooling to a critical temperature. Consequently, the viscoelastic fluid changed to an elastic hydrogel. From the perspective of a microscopic viewpoint, we have demonstrated that elongated wormlike micelles have transformed into large cylindrical structures. In order to better understand the thermo-responsive transition from wormlike micelle to a hydrogel, we investigated the factors that may govern the phase transition in a series of different surfactant–hydrotrope systems.

Firstly, the effect of surfactant chain length on the sol–gel transition was investigated. Fig. 9a gives the profile of gel temperature *versus* NaSal concentration in the system of 40 mM C_{18}MIMBr and 40 mM C_{16}MIMBr. It is interesting to find that extending the surfactant hydrophobic length from C_{16} to C_{18} leads to a remarkable increase of gel temperature (Fig. 9a). On the other hand, the hydrogel from C_{18}MIMBr–NaSal gives well-aligned rigid cylindrical structures and sheets (Fig. 9b), which endows a superior shear modulus to the C_{18}MIMBr–NaSal system compared to the C_{16}MIMBr–NaSal system (Fig. 9c). Hence, it can be concluded that hydrophobic interactions may facilitate the hydrogel formation in this surfactant–hydrotrope system.

Secondly, the nature of the hydrotrope was taken into consideration. We selected four hydrotropes with different hydrophobicities, namely sodium benzoic acid, sodium 2-hydroxybenzoic acid (sodium salicylic acid), sodium 3-hydroxybenzoic acid and sodium 4-hydroxybenzoate. It is known that these four hydrotropes display remarkably different affinities to cationic surfactants.[53–55] Compared to the other hydrotropes, sodium salicylate is the most effective counterion for binding to cationic surfactant headgroups and promoting micelle growth (the bound fraction of salicylate can be as high as 93% by self-diffusion studies[56]). Interestingly, we found that the thermo-responsive sol–gel transition can be only observed in C_{16}MIMBr solutions with NaSal but not with sodium benzoic acid, sodium 3-hydroxybenzoic acid and sodium 4-hydroxybenzoate. Thus we suspected that the strong binding ability of the hydrotrope is an important factor for the occurrence of thermo-responsive hydrogel formation.

Thirdly, the effect of the surfactant headgroup was further explored by replacing the imidazolium-type surfactant with a quaternary ammonium surfactant. Cetyltrimethylammonium bromide is an extensively used quaternary ammonium surfactant. It is meaningful to find that a sol–gel transition can not be detected in a CTAB–hydrotrope solution upon cooling.

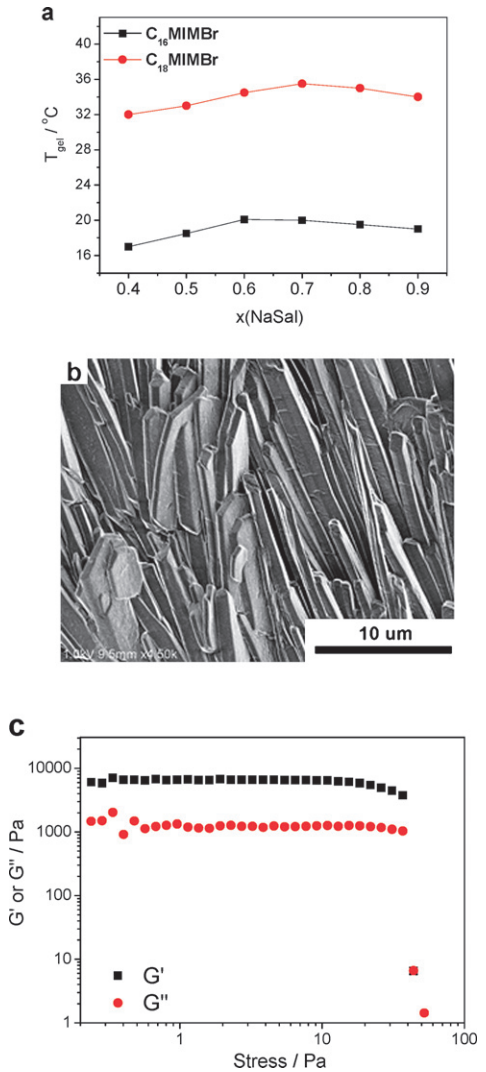

Fig. 9 (a) Profile of gel temperature *versus* NaSal concentration in the systems of 40 mM C_{18}MIMBr and 40 mM C_{16}MIMBr. (b) SEM image of the 40 mM C_{18}MIMBr and 28 mM NaSal xerogel at 34 °C. (c) Dynamic stress sweep of the hydrogel at a frequency of 1 Hz ($T = 20$ °C).

Hence, we speculated that π–π interactions between aromatic groups may play a key role in the thermo-responsive phase transition.

It can be found from the above results that a longer surfactant hydrocarbon chain, strong hydrotrope affinity and an aromatic surfactant headgroup may facilitate the transition from wormlike micelle solution to elastic hydrogel. It is well acknowledged that extending a surfactant's hydrocarbon chain favors the hydrophobic effect and the introduction of an aromatic moiety to a surfactant headgroup can endow an additional π–π interaction between aromatic groups. Both these factors may contribute to strong synergic effect between the surfactant and hydrotrope. Owing to this strong intermolecular interaction, electrostatic repulsion between surfactant headgroups can be screened and low curvature structures, namely elongated wormlike micelles, can be formed. More importantly, due to the strong binding of counterions, the surface charge density of wormlike micelles was greatly eliminated. Consequently, when the temperature was cooled, a process of micelle crystallization occurred which may have originated from the fusion of wormlike micelles. Meanwhile, the crystallization of wormlike micelles generates large cylindrical structures and result in the formation of an elastic hydrogel, in which solvent water was entrapped by the cylindrical structures.

Conclusion

In conclusion, we have reported an unexpected thermo-responsive viscoelastic wormlike micelle solution to elastic hydrogel transition in the novel surfactant–hydrotrope mixture. Above the gel temperature, viscoelastic wormlike micelles can be formed in the surfactant solution. Below the gel temperature, an elastic hydrogel can be formed, which is composed of large cylindrical structures. It is proposed that the viscoelastic solution to hydrogel transition is a result of micelle crystallization which was closely related to the strong interaction between the C_{16}MIMBr and NaSal. The intermolecular interactions between the surfactant and hydrotrope, including electrostatic attraction, the hydrophobic effect and especially the π–π interactions, account for this peculiar phase behavior. We hope this work can shed light on a better understanding of structure–property relationships in surfactant–hydrotrope systems.

Acknowledgements

This work was supported by the National Natural Science Foundation of China (20873001, 20633010 and 50821061) and National Basic Research Program of China (Grant No. 2007CB936201).

References

1 J.-M. Lehn, *Science*, 2002, **295**, 2400.
2 G. M. Whitesides and M. Boncheva, *Proc. Natl. Acad. Sci. U. S. A.*, 2002, **99**, 4769.
3 D. Philp and J. F. Stoddart, *Angew. Chem., Int. Ed. Engl.*, 1996, **35**, 1155.
4 H. W. Jun, S. E. Paramonov and J. D. Hartgerink, *Soft Matter*, 2006, **2**, 177.
5 T. J. Deming, *Soft Matter*, 2005, **1**, 28.
6 S. Svenson, *Curr. Opin. Colloid Interface Sci.*, 2004, **9**, 201.
7 T. Kunitake and Y. Okahata, *J. Am. Chem. Soc.*, 1977, **99**, 3860.
8 J. C. Hao and H. Hoffmann, *Curr. Opin. Colloid Interface Sci.*, 2004, **9**, 279.
9 S. J. Candau, E. Hirsch and R. Zana, *J. Colloid Interface Sci.*, 1985, **105**, 521.
10 M. E. Cates and S. J. Candau, *J. Phys.: Condens. Matter*, 1990, **2**, 6869.
11 M. E. Cates, *J. Phys. Chem.*, 1990, **94**, 371.
12 S. J. Candau, A. Khatory, F. Lequeux and F. Kern, *J. Phys. IV*, 1993, **3**, 197.
13 L. J. Magid, *J. Phys. Chem. B*, 1998, **102**, 4064.
14 C. A. Dreiss, *Soft Matter*, 2007, **3**, 956.
15 S. Ezrahi, E. Tuval and A. Aserin, *Adv. Colloid Interface Sci.*, 2006, **128**, 77.
16 H. Rehage and H. Hoffmann, *Mol. Phys.*, 1991, **74**, 933.
17 L. M. Walker, *Curr. Opin. Colloid Interface Sci.*, 2001, **6**, 451.
18 G. C. Maitland, *Curr. Opin. Colloid Interface Sci.*, 2000, **5**, 301.
19 J. Yang, *Curr. Opin. Colloid Interface Sci.*, 2002, **7**, 276.
20 J. L. Zakin and H. W. Bewersdorff, *Rev. Chem. Eng.*, 1998, **14**, 2553.
21 R. D. Koehler, S. R. Raghavan and E. W. Kaler, *J. Phys. Chem. B*, 2000, **104**, 11035.

22 S. R. Raghavan, G. Fritz and E. W. Kaler, *Langmuir*, 2002, **18**, 3797.
23 B. A. Schubert, E. W. Kaler and N. J. Wagner, *Langmuir*, 2003, **19**, 4079.
24 A. Bernheim-Groswasser, E. Wachtel and Y. Talmon, *Langmuir*, 2000, **16**, 4131.
25 K. Imanishi and Y. Einaga, *J. Phys. Chem. B*, 2007, **111**, 62.
26 D. P. Acharya, S. C. Sharma, C. Rodriguez-Abreu and K. Aramaki, *J. Phys. Chem. B*, 2006, **41**, 20224.
27 H. Hoffmann, A. Rauschera, M. Gradzielski and S. F. Schulz, *Langmuir*, 1992, **8**, 2140.
28 P. Fischer, H. Rehage and B. Gruning, *J. Phys. Chem. B*, 2002, **106**, 11041.
29 R. Kumar, G. Kalur, L. Ziserman, D. Danino and S. Raghavan, *Langmuir*, 2007, **23**, 12849.
30 P. A. Hassan, S. R. Raghavan and E. W. Kaler, *Langmuir*, 2002, **18**, 2543.
31 S. Imai and T. Shikata, *J. Colloid Interface Sci.*, 2001, **244**, 399.
32 K. Bijma, M. J. Blandamer and J. B. F. N. Engberts, *Langmuir*, 1997, **13**, 4843.
33 C. Oelschlaeger, G. Waton and S. J. Candau, *Langmuir*, 2003, **19**, 10495.
34 R. Abdel-Rahem, M. Gradzielski and H. Hoffmann, *J. Colloid Interface Sci.*, 2005, **288**, 570.
35 T. K. Hodgdon and E. W. Kaler, *Curr. Opin. Colloid Interface Sci.*, 2007, **12**, 121.
36 M. Singh, C. Ford, V. Agarwal, G. Fritz, A. Bose, V. T. John and G. L. McPherson, *Langmuir*, 2004, **20**, 9931.
37 L. M. Zhai, B. Herzog, M. Drechsler and H. Hoffmann, *J. Phys. Chem. B*, 2006, **110**, 17699.
38 R. T. Buwalda, M. C. A. Stuart and J. B. F. N. Engberts, *Langmuir*, 2000, **16**, 6780.
39 D. Grabner, L. Zhai, Y. Talmon, J. Schmidt, N. Freiberger, O. Glatter, B. Herzog and H. Hoffmann, *J. Phys. Chem. B*, 2008, **112**, 2901.
40 K. Horbaschek, H. Hoffmann and C. Thunig, *J. Colloid Interface Sci.*, 1998, **206**, 439.
41 L. Wattebled and A. Laschewsky, *Langmuir*, 2007, **23**, 10044.
42 T. Lu, J. B. Huang, Z. H. Li, S. K. Jia and H. L. Fu, *J. Phys. Chem. B*, 2008, **112**, 2909.
43 B. Dong, N. Li, L. Q. Zheng, L. Yu and T. Inoue, *Langmuir*, 2007, **23**, 4178.
44 B. Dong, X. Zhao, L. Q. Zheng, J. Zhang, N. Li and T. Inoue, *Colloids Surf. A*, 2008, **317**, 666.
45 B. Chamiot, C. Rizzi, L. Gaillon, J. Sirieix-Plenet and J. Lelievre, *Langmuir*, 2009, **25**, 1311.
46 E. Cappelaere and R. Cressely, *Rheol. Acta*, 2000, **39**, 346.
47 V. Croce, T. Cosgrove, G. Maitland, T. Hughes and G. Karlsson, *Langmuir*, 2003, **19**, 8536.
48 A. Khatory, F. Kern, F. Lequeux, J. Appell, G. Porte, N. Morie, A. Ott and W. Urbach, *Langmuir*, 1993, **9**, 933.
49 S. R. Raghavan, H. Edlund and E. W. Kaler, *Langmuir*, 2002, **18**, 1056.
50 T. Shikata, H. Hirata and T. Kotaka, *Langmuir*, 1998, **4**, 354.
51 S. J. Bachofer, U. Simonis and T. A. Nowicki, *J. Phys. Chem.*, 1991, **95**, 480.
52 M. Vermather, P. Stiles, S. J. Bachofer and U. Simonis, *Langmuir*, 2002, **18**, 1030.
53 V. K. Aswal, *J. Phys. Chem. B*, 2003, **107**, 13323.
54 A. L. Underwood and E. W. Anacker, *J. Phys. Chem. B*, 1984, **88**, 2390.
55 A. R. Rakitin and George R. Pack, *Langmuir*, 2005, **21**, 837.
56 U. Olsson, O. Soderman and P. Guering, *J. Phys. Chem.*, 1986, **90**, 5223.